Mon. Not. R. Astron. Soc. **370,** 1859–1866 (2006) doi:10.1111/j.1365-2966.2006.10609.x

Swift observations of GRB 050712

Massimiliano De Pasquale,[1]★ Dirk Grupe,[2] T. S. Poole,[1] A. A. Breeveld,[1] S. Zane,[1] S. R. Rosen,[1] M. J. Page,[1] K. O. Mason,[1] D. N. Burrows,[2] H. A. Krimm,[3,4] N. Gehrels,[3] J. A. Nousek,[2] P. W. A. Roming,[2] S. Kobayashi[5] and B. Zhang[6]

[1]*Mullard Space Science Laboratory, University College London, Holmbury St. Mary, Dorking, Surrey RH5 6NT*
[2]*Department of Astronomy and Astrophysics, Pennsylvania State University, 525 Davey Laboratory, University Park, PA 16802, USA*
[3]*NASA/Goddard Space Science Flight Center, Greenbelt, MD 20771, USA*
[4]*Universities Space Research Association, Columbia, MD 21044, USA*
[5]*Astrophysics Research Institute, Liverpool John Moore University, Twelve Quays House, Birkenhead CH4 1LD*
[6]*Department of Physics, University of Nevada, Las Vegas, NV 89154, USA*

Accepted 2006 May 23. Received 2006 May 22; in original form 2005 December 20

ABSTRACT

We present the results of X-ray and optical observations of GRB 050712 performed by *Swift*. The X-ray light curve of this burst exhibits episodes of flares in the first 1000 s, the same epoch at which the UVOT detected an optical counterpart. A shallow X-ray decay, with a decay slope of $\alpha = -0.73$, followed and lasted $\sim$70 ks. This behaviour can be explained in terms of activity of the gamma-ray burst 'inner engine', with the possibility that the last flare is caused by the interaction of the ejecta with the surrounding medium.

We also find interesting spectral parameters for the X-ray emission. In particular, data suggest the presence of an intrinsic absorption in the first 1000 s, which can be explained if circumburst medium clouds lie along the line of sight.

Key words: gamma-rays: bursts.

1 INTRODUCTION

Follow-up observations of gamma-ray bursts (GRBs) have shown that the initial prompt emission is followed by an afterglow, i.e. a fading X-ray, optical and radio source that can last up to several months after the γ-ray flash. According to the currently accepted theory, the afterglow arises when the burst ejecta interact with the surrounding medium and produce a shock, which propagates in the medium and heats the electrons. The latter, cooling down through synchrotron emission, produce the observed radiation. Studies of afterglows can thus provide invaluable information on the central engine of GRBs, on the circumburst medium and can possibly lead to the identification of different subclasses in the GRB population.

Until recently, most follow-up observations did not start until a few hours after the GRB, when the afterglow had already faded significantly. This situation has changed with the launch of the *Swift* mission, which provides both a rapid alert of GRB triggers to ground-based observers, and rapid (within $\sim$1 min after the γ-ray trigger) X-ray and optical/UV follow-up observations of the burst afterglow. The temporal behaviour of the GRB emission at this early epoch has been thus unveiled. Several interesting features have been discovered (see Burrows et al. 2005b; Roming et al. 2005; Nousek et al. 2006; Zhang et al. 2006, for detailed discussions): (i) the typical behaviour of the X-ray emission has been shown to consist of an initial steep decay, followed by a shallow one about 100–1000 s after the trigger; (ii) a second change of the decay slope usually occurs about 10 ks later and (iii) in some cases, a further steepening of the slope, typical signature of collimated outflow, is observed 100–1000 ks after the trigger. Furthermore, in a few events the initial fast decay was unobserved, and in others X-ray flares have been detected, superimposed on this 'template' time behaviour (e.g. Burrows et al. 2005b). As for the optical emission, it has been observed that in many cases the optical/UV emission is much lower than expected (Roming et al. 2005), suggesting some cause of suppression of the flux in the optical band.

Even in past years, irregular temporal features have been occasionally seen in various bursts (see Zhang & Mészáros 2002b, and references therein): just to mention some examples these include a rebrightening in GRB 970508, GRB 021004 and step-like features in GRB 030309. Other similar peculiarities have been observed in several cases (e.g. GRB 970228, GRB 980326, GRB 000203C). Various interpretations have been proposed, mainly in terms of 'refreshed shocks" (Panaitescu, Mészáros & Rees 1998), supernova components (Bloom et al. 1999; Reichart 1999; Galama et al. 2000), dust echoes (Esin & Blandford 2002) or microlensing (Garnavich, Loeb & Stanek 2000). On the other hand, signatures detected by *Swift* in the GRB light curve at earlier times may provide diagnostic

★E-mail: mdp@mssl.ucl.ac.uk

about the nature of the injection and eventually probe whether the energy is released impulsively during the event or more continuously during the immediate post-burst epoch (see e.g. Zhang & Mészáros 2002b), eventually with different Lorentz factors of the ejecta (Panaitescu et al. 2005).

In this paper, we report the properties of the *Swift* GRB 050712, and discuss them in the context of the current models and scenarios of GRBs. In Section 2, we describe the analysis of γ and X-ray data, while the analysis of UltraViolet Optical Telescope (UVOT) data is shown in Section 3. The possible interpretations are examined in Section 4 and we finally summarize our conclusions in Section 5.

2 ANALYSIS OF THE γ-RAY AND X-RAY DATA

The *Swift* observatory (Gehrels et al. 2005) carries three science instruments: the Burst Alert Telescope (BAT; Barthelmy et al. 2005), which locates GRBs with 3-arcmin accuracy, the narrow field X-ray telescope (XRT, Burrows et al. 2005a) and the UVOT (Roming et al. 2005). When BAT detects a GRB trigger, *Swift* slews towards the source position within a few tens of seconds.

GRB 050712 triggered the BAT instrument at 14:00:28 UT on 2005 July 12, (Grupe et al. 2005a). The refined BAT position is RA $= 05^h\ 10^m\ 48^s$, Dec. $= 64^\circ\ 55'\ 48.2''$ with a position uncertainty of $1.7'$ (90 per cent confidence level, Krimm, private communication; Markwardt et al 2005). The γ-ray band emission started 8 s before the BAT trigger time and the light curve shows a very broad peak (see Fig. 1), with a peak count rate of $\sim$500 counts s^{-1} (Grupe et al. 2005a).

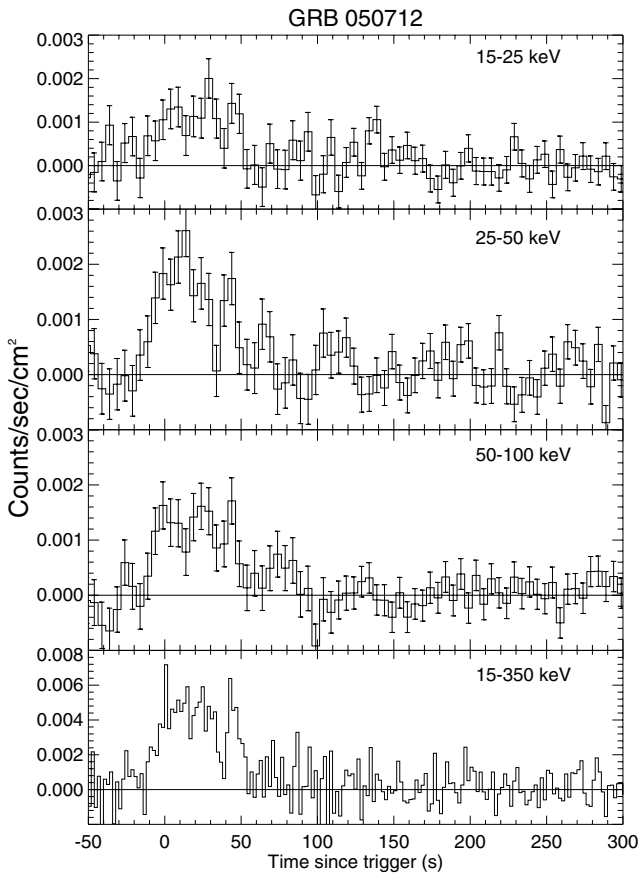

Figure 1. GRB 050712 BAT light curve.

From the analysis of the BAT data (15–350 keV energy band), we found that the GRB duration is $t_{90} = 48$ s. For the spectral analysis, we report results obtained in the 15–150 keV band, because the mask-weighted technique has been used to subtract the background. Above 150 keV, the coded mask becomes transparent and the mask-weighting technique is no longer effective. A single power law provides a satisfactory fit [$\chi^2_\nu = 62.8$ for 57 degrees of freedom (d.o.f.)] of the BAT spectrum, with an energy index of $\beta = -0.49 \pm 0.11$ (hereafter we will assume the convention $F_\nu \propto t^\alpha \nu^\beta$, where α is the decay slope and β is the spectral index; errors are reported at 1σ confidence level, unless specified otherwise). The corresponding fluence is $(1.10 \pm 0.07) \times 10^{-6}$ erg cm^{-2} s^{-1} (15–150 keV band).

XRT and UVOT observations started $\sim$160 s and $\sim$164 s after the trigger, respectively. Initially, the source was not bright enough for the XRT to perform an onboard centroid (Falcone et al. 2005a). Subsequent analysis showed the presence of an unknown X-ray source, with refined coordinates of R.A. $= 05^h\ 10^m\ 47.7^s$, Dec. $= 64^\circ\ 54'\ 48.2''$, with a $6''$ radius error circle (90 per cent confidence level). This position is within $62''$ of the initial BAT position (Grupe et al. 2005b). This source subsequently faded, indicating that it was the X-ray counterpart of GRB 050712. XRT data used in this paper were initially taken in windowed timing (WT) mode (Hill et al. 2004), and subsequently in photon counting (PC) mode.

The XRT data were reduced with the XRTPIPELINE software, version 0.9.9. Source and background photons of the WT mode data were selected by XSELECT version 2.3 in a box with a length of 34.5 pixels (= 81 arcsec). The source photons of the PC mode data were selected in a circular region with a radius of $r = 47$ arcsec and the background photons in a nearby circular region with a radius of $r = 96$ arcsec. For the spectral data events with grades 0–2 and 0–12 were selected for the WT and PC mode data, respectively. For the PC mode data of the first orbit, because of pileup, the inner 5 arcsec of the circle had to be discarded from the spectral analysis. The spectral data were re-binned by GRPPHA 3.0.0 with 20 photons per bin. The spectra were analysed using XSPEC version 12.2.1. The auxiliary response files were created with XRTMKARF and the standard response matrices swxwt0to2_20010101v007.rmf and swxpc0to12_20010101v007.rmf were used for the WT and the PC data, respectively.

The background-subtracted X-ray light curve in the 0.3–10.0 keV energy range was constructed by using the ESO Munich Image Data Analysis Software MIDAS (version 04Sep). The binning was dynamically performed. At the beginning of the observations, the binning was set to 50 photons per bin while at later times it was reduced to 10 photons per bin. A pileup correction for the PC mode data of the first orbit was applied as described in Nousek et al. (2006). Count rates were converted into fluxes by determining the energy conversion factors for the PC and WT mode data as described by Nousek et al. (2006).

In order to search for spectral variability through out the observations we also derived the temporal behaviour of the hardness ratio. The hardness ratio has been calculated as HR $= (H - S)/(H + S)$, where S and H are the number of counts in the 0.3–1.0 and 1.0–10.0 keV bands, respectively.

Figs 2 and 3 show the X-ray light curve in the 0.3–10 keV energy band. The presence of three flares is evident, about 210, 240 and 480 s after the BAT trigger. We also tested if the flares were visible in the late BAT data. A visual inspection of the light curve reported in Fig. 1 shows no obvious flare at these epochs. Thus we looked at the data with a statistical approach. We set up a script to go through the phase space of energy bands and time-intervals (from $t + 210$ to $t + 280$ s) and made a set of 160 sky images, each of which we

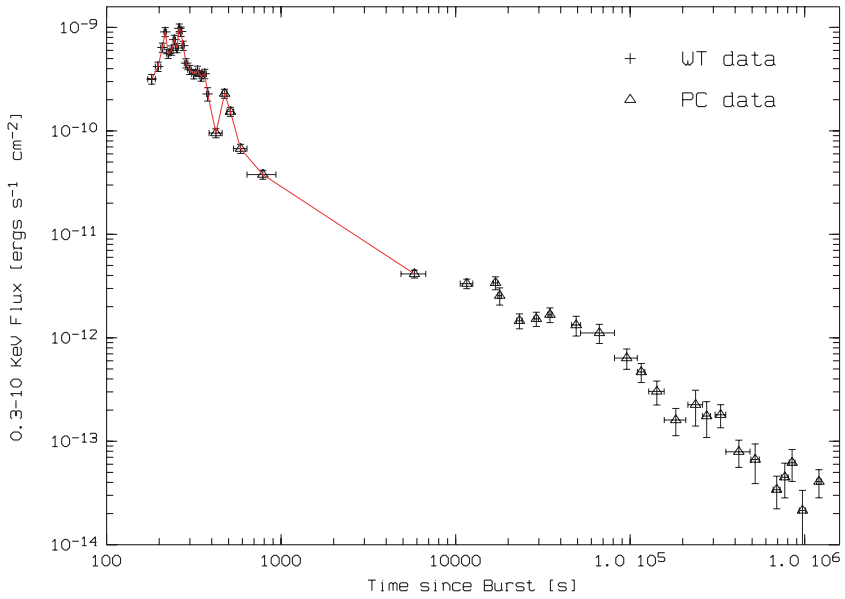

Figure 2. X-ray light curve of GRB 050712 detected with the *Swift* XRT in the 0.3–10 keV band. Data points of the first 1000 s are connected to show the flares at 210, 280 and 480 s more clearly.

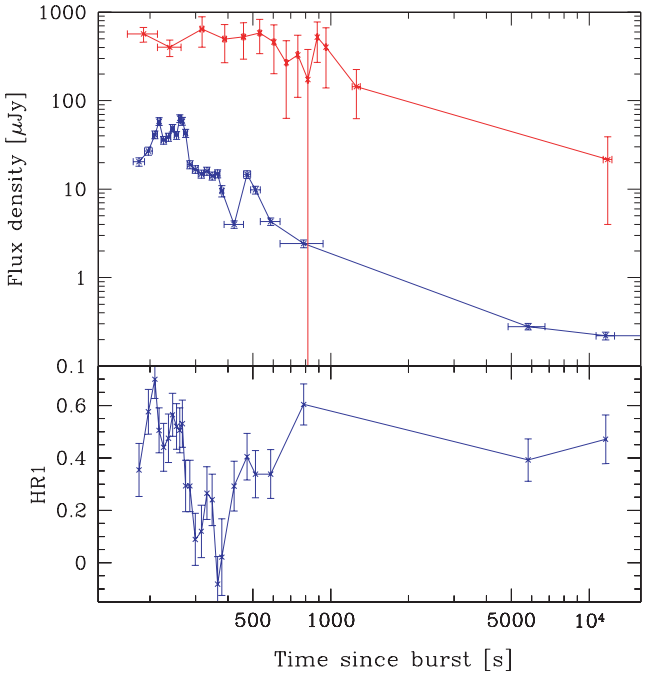

Figure 3. Top panel: zoom of the first 5000-s *Swift* GRB 050712 with XRT (0.3–10 keV, blue line) and UVOT (*V* filter, red line). Bottom panel: hardness ratio evolution in the X-ray band. The hardness ratio is defined by HR = $(H - S)/(H + S)$, where S and H are the counts in the 0.3–1.0 and 1.0–10.0 keV bands, respectively.

checked for flux at the source position. Out of the 160 trials we see 58 cases with a significance of $>2.0\sigma$, far more than we expect from statistics. The most significant single trial was in the interval 25–50 keV, $t + 250$ –$t + 260$ s, at 4σ. However, if we look at the whole time-interval and energy band ($t + 240$–$t + 280$ s and 15–150 keV), the significance is only 2.0σ ($t + 240$–$t + 280$ s in 25–50 keV gives 2.9σ). Therefore, the evidence for this peak is larger in the soft band with respect to the total one. To make sure that there was no systematic bias, we did a similar test using a time-interval before the burst and we found a distribution consistent with statistics.

Between the second and third flares, the light curve exhibits a plateau which lasts approximately for 50 s, followed by a steep decline and then by a fast rise. After the third flare, which lasts for about 200 s, there is a gap in the coverage due to the *Swift* orbit, thus we cannot constrain the behaviour of the X-ray light curve during this interval. However, an extrapolation of the later X-ray light curve backward reconnects to the late points of the flare, showing a shallow decline after ∼500 s and a possible break at later times, i.e. around 70 ks after the trigger (see further).

We note that the 0.3–10 keV fluence in the first 1000 s (i.e. in the interval including the three flares) is $\approx 9 \times 10^{-8}$ erg cm^{-2}, i.e. ∼10 per cent of the fluence detected in the 15–150 keV band during the prompt emission phase.

We fitted the X-ray spectra taken at different time-intervals with an absorbed power law. Best-fitting values of column density and energy spectral index are summarized in Table 1, while Fig. 3 shows the evolution of the hardness ratio. Spectra taken before, during and after the flares are shown in Fig. 4. As we can see, the X-ray data indicate a clear spectral evolution throughout the first 1000 s, with a change in the spectral index. In particular, after the first ∼200–300 s the spectrum starts softening monotonically, while, after the second peak, it changes abruptly and the energy index increases up to a value consistent with that observed in the late phases of the afterglow.

We also detect a photoelectric absorption in excess of the Galactic column density, $N_{\rm H}^{\rm Gal} = 0.13 \times 10^{22}$ cm^{-2} (Dickey & Lockman 1990). Further discussion on this issue is postponed to Section 4.3.

3 OPTICAL OBSERVATIONS BY UVOT IN THE UV/OPTICAL

Swift UVOT detected the optical counterpart of GRB 050712 in the *V* band, ∼200 s after the BAT trigger (Rol et al. 2005). The source

Table 1. Values of the best-fitting parameters for the spectral fit of GRB 050712 X-ray afterglow. Data have been divided into four temporal sections: WT data before the second flare, WT data after the second flare, PC data at the third flare, and PC data taken during the late afterglow. The column density reported in the table is the intrinsic one, calculated for two different values of the redshift, $z = 1$ and 2 (an additional contribution due to the Galactic column density has been fixed assuming $N_{\rm H}^{\rm Gal} = 1.3 \times 10^{21}$ cm^{-2}, Dickey & Lockman 1990). Errors are at 68 per cent confidence level, χ^2_ν/(d.o.f.) is for the $z = 1$ case.

Section(s after trigger)	β	$N_{\rm H} \times 10^{21}$ cm^{-2} at $z = 1$	$N_{\rm H} \times 10^{21}$ cm^{-2} at $z = 2$	χ^2_ν/(d.o.f.)
160–281	$-1.10^{+0.16}_{-0.17}$	$5.60^{+2.40}_{-2.10}$	$15.2^{+3.96}_{-3.45}$	21.5/23
281–350	$-1.71^{-0.21}_{+0.18}$	$1.88^{+1.79}_{-1.15}$	$5.26^{+4.85}_{-3.20}$	37.3/25
440–1050	$-1.16^{+0.18}_{-0.20}$	$1.65^{+2.01}_{-1.00}$	$4.34^{+5.39}_{-2.63}$	12.1/15
5000–1.2e6	$-0.96^{+0.23}_{-0.25}$	$1.30^{+6.50}_{-5.85}$	$3.88^{+19.40}_{-16.65}$	4.4/7

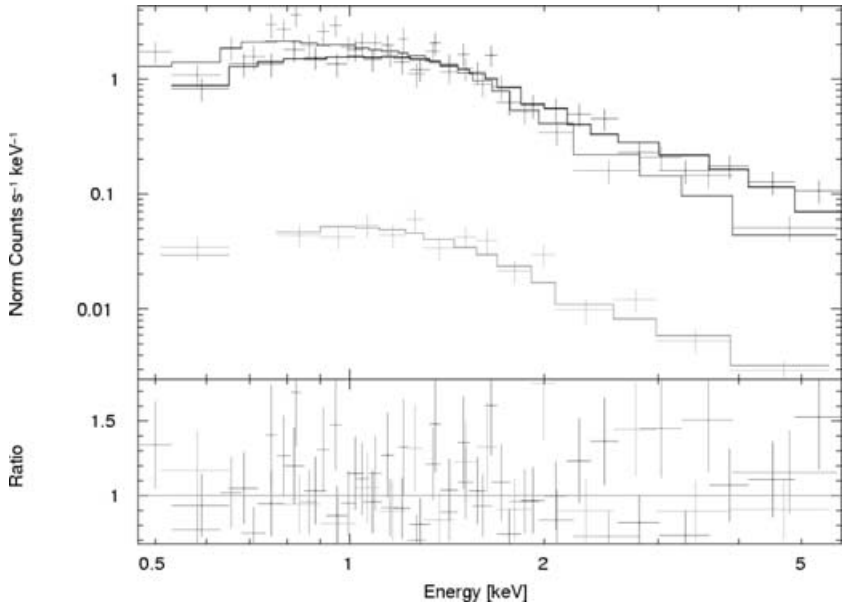

Figure 4. Evolution of the XRT spectrum during the first 1050 s from the BAT trigger. Dark grey line: WT spectrum at the first and second flare (205–281 s). Grey line: WT spectrum after the second flare (281–350 s). Light grey line: PC data (450–1050 s). Data points and best-fitting model are shown in the top panel, while residuals are shown in the bottom panel.

was fading away, but has been positively detected by *Swift* UVOT until 15000 s after the trigger. The log of optical observations is reported in Table 2.

The analysis of the *Swift* UVOT optical images was performed by correcting for attitude drifts with an in-house software and summing up all the exposures in the indicated time-interval with UVOTIMSUM, part of SWIFT software version 2.0.[1] Source counts were extracted in a circular region of 3-arcsec radius, while the background was extracted in a circular region of 20-arcsec radius. In both the cases, the packages[2] DS9 version 4.0 and XIMAGE version 4.3.1 were used to create the region files and extract counts, respectively. Counts were converted in magnitudes by using the latest CALDB zero-points, *swuphot20041120v102.fits*.[3] UVOT magnitudes can be equated to the Johnson standard.

The *V*-band light curve is shown in Fig. 3. A positive detection has also been obtained in the *U* band by UVOT (see Table 2 for values). This allows us to put an upper limit on the redshift of GRB 050712. For redshift $z = 3$, the intervening extragalactic hydrogen would produce a $U - V$ colour index of $\simeq$1.5 (Zuo & Lu 1993; Lamb & Reichart 2000; Lamb 2003) and we would not expect an optical detection in the *U* band at all for redshift larger than this value. Rather, our data suggest that magnitudes in the *V* and *U* band are equal within errors. We can therefore take $z = 3$ as upper limit for the redshift of GRB050712.

For completeness, we also list two successful ground-based optical follow-up observations which were triggered by the prompt *Swift* localization and led to the detection of the optical afterglow in the *R* band between 8 and 14 h after the burst trigger (Maiorano et al. 2005; Zeh et al. 2005).

4 DISCUSSION

4.1 X-ray flares

As discussed in Section 2, the X-ray light curve of GRB 050712 exhibits at least three flares, at about 210, 240 and 480 s after the BAT trigger. These features have been observed with *Swift* in several other GRBs (see Burrows et al. 2005b; Falcone et al. 2005b; Romano

[1] http://swift.gsfc.nasa.gov/docs/swift/analysis.
[2] http://heasarc.gsfc.nasa.gov/docs/software.
[3] http://swift.gsfc.nasa.gov/docs/heasarc/caldb/data/swift/uvota.

Table 2. Log of GRB 050712 optical observations. Values quoted in this table have been corrected for Galactic extinction. *U* and *V* results come from the *Swift* UVOT, while the two *R*-band measurements have been performed by Zeh et al. (2005) (Tautenburg) and Maiorano et al. (2005) (Bologna Observatory).

Time after GRB (s)	Magnitude	Band
164–214	$17.81^{+0.23}_{-0.19}$	*V*
214–264	$18.19^{+0.25}_{-0.21}$	*V*
311–321	$16.86^{+0.51}_{-0.35}$	*V*
383.5–393.5	$17.14^{+0.66}_{-0.41}$	*V*
457.5–462.5	$17.08^{+0.63}_{-0.40}$	*V*
526.5–536.5	$16.97^{+0.59}_{-0.38}$	*V*
597.5–607.5	$17.23^{+0.76}_{-0.44}$	*V*
668.5–678.5	$17.82^{+1.57}_{-0.62}$	*V*
740.5–750.5	$17.59^{+1.22}_{-0.56}$	*V*
811.5–821.5	$19.09^{+\infty}_{-0.86}$	*V*
882.5–892.5	$17.09^{+0.72}_{-0.43}$	*V*
954–964	$17.38^{+1.16}_{-0.55}$	*V*
1210–1300	$18.50^{+0.92}_{-0.49}$	*V*
11 354–12 254	$20.57^{+1.88}_{-0.65}$	*V*
282.5–292.5	$17.35^{+0.74}_{-0.44}$	*U*
353.5–363.4	>20.25	*U*
425–435	$17.46^{+0.90}_{-0.48}$	*U*
496.5–506.5	$17.77^{+1.24}_{-0.57}$	*U*
567.5–577.5	$18.02^{+1.83}_{-0.65}$	*U*
639–649	$18.58^{+\infty}_{-0.92}$	*U*
710.5–720.5	$17.55^{+1.02}_{-0.52}$	*U*
781.5–791.5	$18.65^{+\infty}_{-0.98}$	*U*
852.5–862	$17.95^{+2.40}_{-0.69}$	*U*
924–934	$18.97^{+1.44}_{-0.60}$	*U*
1001.5–1101.5	$18.19^{+0.49}_{-0.33}$	*U*
6477.5–7140	$20.02^{+1.24}_{-0.56}$	*U*
30 500	20.08 ± 0.4	*R*
51 900	20.73 ± 0.05	*R*

et al. 2006; Zhang et al. 2006) and seem to be characteristic of the X-ray emission detected at early times.

In principle, the occurrence of flares can be associated with several mechanism such as: reverse shock propagation, presence of high-density clouds surrounding the progenitor, or GRB emission collimated in a multicomponent outflow with variable amount of energy per solid angle, as in models involving 'structured jets' or 'patchy shells' (Kumar & Piran 2000; Berger et al. 2003; Huang et al. 2004).

However, the majority of these models, which ultimately account for different ways in which the ejecta interact with the circumbust medium, cannot account for the rapid onset and decline of the X-ray flare observed in several GRBs by *Swift* (Zhang et al. 2006). An alternative scenario for these features is that the 'inner engine' of the GRBs does not switch off at the end of the main high-energy event but it still emits shells, which continue to collide and produce radiation. Following Zhang & Mészáros (2002a), in this case the peak energy of the flare emission, $E_{\rm p}$, scales as:

$$E_{\rm p} \propto L^{1/2}\Gamma^{-2}\delta t^{-1}, \quad (1)$$

where L is the luminosity, Γ is the Lorentz factor and δt is the variability time-scale of the flare. The observed X-ray peaks have luminosity lower than that of the main event, and their fluctuations take place on a large time-scale. Also, it is expected that the environment tends to be cleaner so that Γ may be larger. Therefore, late 'internal shocks' can give rise to (X-ray) bursts which are softer as compared with the prompt (γ-ray) emission. The high Lorentz factor of the shells naturally explains fast variations of the flux, in terms of a pure propagation effect. Let us assume that the shells, moving at a dimensionless velocity β, emit a photon at the time $\overline{t_1}$ at a certain distance from the centre of the explosion $\overline{r_1}$ and a second photon at the time $\overline{t_2}$ and position $\overline{r_1}+{\rm d}r$). The time $\bar{t}$ is measured in the Earth observer's reference frame, and the distance between this observer and the shell location is D. This first photon arrives at the observer at the time $t_1 = \overline{t_1} + D/c$, while the second one arrives at a time $t_1 = \overline{t_2} + D/c - \beta\,{\rm d}\bar{t}$ where ${\rm d}\bar{t} = \overline{t_2} - \overline{t_1} \simeq {\rm d}r/c$. In turn, the interval for the observer to receive the two photons is much reduced, i.e. ${\rm d}t = t_2 - t_1 = (1-\beta)\overline{{\rm d}t} \simeq {\rm d}\bar{t}/2\Gamma^2 = {\rm d}r/2\Gamma^2 c$.

In the case at hand, the second flare flux (extrapolated in the 0.3–150 keV band) is $L_{\rm F} \approx 6 \times 10^{-10}$ erg s^{-1} cm^{-2}, the Lorentz Factor should be as high as $\Gamma \approx 1000$ (see Zhang et al. 2006, and reference therein) and the time-scale of variation is 40 s. The corresponding quantities during the prompt emission are $\sim 3 \times 10^{-8}$ erg s^{-1} cm^{-2}, $\Gamma \approx 300$ and $\sim$10 s. For such values, equation (1) predicts a peak energy a factor of $\approx$300 lower than that in the prompt phase. A good measurement of the peak energy of the prompt emission of this burst is unavailable, but if we assume a standard value of 250 keV (Preece et al. 2000), we can infer that the peak energy of the second flare must be at $\approx$1 keV, i.e. in the XRT band.

During the decay of flares produced by late 'internal shocks', the relationship between the spectral and decay indices is given by (Kumar & Piran 2000):

$$\alpha = \beta - 2 \quad (2)$$

provided that the decay slope is computed by re-setting the zero-point time t_0 at the time of the peak (see Zhang et al. 2006, and references therein). We note that several *Swift* bursts exhibit a rapid decay during the early phase of the observed X-ray emission (first hundreds of seconds after the trigger), with spectral slope ~ -1 and decays slope ~ -3, respectively, in agreement with the predictions of equation (2).

In the case of GRB 050712, we found that the X-ray spectral evolution of the emission in the first 400 s is in general agreement with this 'late internal shocks' scenario. During this phase the X-ray spectrum of GRB 050712 softens, with the energy index decreasing from -1.1 to -1.7. This is reminiscent of the behaviour of the prompt emission. For comparison, the spectral index of the low-energy part of the γ-ray emission detected by BAT is around -0.5. Assuming that the first two flares have a similar $t_0 = 180$ s, we get $\alpha = -2.5 \pm 0.6$ and -3.6 ± 0.77 for their decay slopes. We also have $\beta \sim -1.1$ and $\sim$1.7 (see Table 1) for the spectral index of the first and second peak. So our results are in agreement with equation (2). Also, we may speculate that the decay phase observed around $\sim$400 s after the trigger might follow a further release of energy which is not observed as a 'flare' since it is superimposed on that of the first peak. In this case, it would be difficult to fix t_0 properly. However, we find that taking $t_0 = 240$ s gives a decay slope of $\alpha = -3.4 \pm 0.4$, which again satisfies equation (2) (since during this phase the spectral index is the same as before, i.e. $\beta \sim -1.7$).

However, the situation may differ as far as the third X-ray flare, observed at $\sim$480 s, is concerned. First, if this peak were due to a further internal shock occurring in the fireball, then it would be

followed by a fast decay. The rise of this peak is clearly visible at $t = 440$ s after the trigger. Assuming this value for t_0 gives a decay slope of $\alpha = -0.86 \pm 0.02$ which, combined with an energy spectral index of $\beta \sim -1.16$, does not satisfy equation (2). The situation does not improve by choosing slightly different values of t_0. Secondly, the spectrum of the third peak differs ($\sim 4 - 5\sigma$) from that of the previous phase, which could suggest a different origin, while it is much more in agreement with that observed during the late phases of the X-ray afterglow. Late internal shocks might still be responsible for the third flare if, for instance, the emission does not stop suddenly after this peak and other weak flares are released superimposing on the decaying part. In this case, the decay would be shallower than that predicted by equation (2). Moreover, collisions of different shells may well produce emission with diverse spectral properties, and the rapid increase of flux in the third flare, by a factor of $\sim$3 within $\sim$50 s, supports the internal shock scenario.

It should be noted that the behaviour of GRB 050712 X-ray afterglow is rather uncommon. Flare spectra usually soften until they reach the relatively soft afterglow. In this case, the first flare is quite soft, but then the spectrum hardens at later times. However, the spectrum of the last flare is similar to that of the late afterglow, which is hard as compared with other afterglows of other GRBs.

An alternative possibility is that with the third flare we witness the onset of the standard afterglow, i.e. the creation of an 'external shock' when the fireball runs into the circumburst medium. The standard afterglow model predicts that, as a shell of ejecta interacts with the circumburst medium, it gives rise to a 'forward shock', which propagates outward, and to a 'reverse shock', which moves inward through the ejecta (Mészáros & Rees 1997). During this phase, the observable characteristics depend on the dynamical conditions of the fireball.

Two regimes can be identified depending on the 'thickness' of the fireball (Sari & Piran 1999, hereafter SP99). The difference between the two cases is whether a reverse shock becomes relativistic in the frame of unshocked material during its crossing of the shell. If this happens, the shell is defined as 'thick'. Otherwise, the shell is defined as 'thin'. In the case of a thin shell, SP99 have shown that the evolution of the afterglow is well described by a power-law decay if the time is measured starting from the explosion time, which is a good approximation of the time at which the first photons are collected. The situation differs if the shell is 'thick', i.e. if

$$\Delta > \left(\frac{E}{n m_{\rm p} c^2}\right)^{1/3} \gamma^{-8/3}, \qquad (3)$$

where Δ is the initial thickness of the shell in the observer frame, γ and E are its initial Lorentz factor and kinetic energy, n is the number of particles of the circumburst medium per unit volume, and $m_{\rm p}$ is the proton mass. If we assume typical parameters of $E \sim 10^{52}$ erg, $n = 10$ cm^{-3} (see Berger et al. 2003) and consider that $\Delta = cT$, where T is the burst duration, we need to have $\gamma > 70$, which is easy to satisfy (see, however, Zhang & Mészáros 2004). Most of the energy is released into the surrounding material only when the shell has been crossed by the reverse shock. Following again SP99 (see also Galli & Piro 2005; Piro et al. 2005), this happens after a time $t_\Delta \sim \Delta/c$, roughly similar to the burst duration. Only from the time t_Δ onward, the deceleration of the shell scales as $\gamma^{-3/8}$, in a self-similar manner, and the afterglow decay can be fitted by a power-law (or broken power law) model.

Quite interestingly, we find that this might the case of GRB 050712. By rescaling the zero-time to $t_\Delta = 440$ s (i.e. to the onset of the third peak), we find that a broken power-law model provides an acceptable fit of the light curve at $t \geqslant t_\Delta$, with $\chi^2_\nu = 33.7$ for 23 d.o.f. (see Fig. 5), which is acceptable at 7 per cent confidence level. The best-fitting parameters are $\alpha_1 = -0.73 \pm 0.01$, $\alpha_2 = -1.23^{-0.10}_{+0.07}$ for the two decay slopes before and after the break, and $t_{\rm break} = 66240^{+25000}_{-10300}$ s. The presence of a break is statistically significant since a fit with a single power law gives $\chi^2_\nu = 93$ for 25 d.o.f.

The comparison between the optical and X-ray light curve is also illuminating. First of all, in the optical we do not see the strong variability that is present in the X-ray light curve. We have tried to fit the UVOT V data points with a rescaled X-ray light curve in the first 10 000 s, and we have obtained a $\chi^2 = 38.5$ for 13 d.o.f. Therefore, the probability that the two light curves are consistent is only 5×10^{-4}. The major differences in the two light curves arise from the first part. In the V-band light curve we see no increase correspondent to the first and second X-ray flares, no decrease at the time of the steep decay at $\sim$400 s, and again no increase at the time of the rise of the third flare. Rather, the optical light curve in the first 500 s is fully compatible with being constant: a fit with a constant gives $\chi_\nu = 1.6/4$. This suggests that the origin of the optical emission is different from that of the X-ray. A possible origin for the optical emission would be 'reverse shocks' crossing the ejecta inwards, as already suggested in the case of GRB 990123 and GRB 021211 Zhang & Mészáros 2004. Reverse shocks are mild-relativistic, so their emission is not expected to be associated with very fast fluctuations of the radiation, as in case of internal shocks. After it reaches the peak, reverse shock emission is usually expected to fade away with a power-law decay $F \propto t^{-2}$, and it has been shown by several authors (see Kobayashi et al. 2000; Zhang, Kobayashi & Mészáros 2003; Zhang & Kobayashi 2005) that, if ejecta are magnetized and the optical band is below the synchrotron cooling frequency, the peak itself may be broad and the slope more gentle, $F \propto t^{-1/2}$. Furthermore, the emission from the reverse shock may well overlap that of the forward shock component after the forward shock peak time (GRB 021211 may be a marginal such case, see Zhang et al. 2003). In the case at hand, we see a decrease in the optical starting 500 s after the trigger, roughly after the peak in the X-ray. The optical-to-X-ray energy index $\beta_{\rm OX}$ fluctuates until $\sim$500 s after the trigger, when it stabilizes at $\beta_{\rm OX} = -0.8$, remaining consistent with this value for the rest of the afterglow. These clues suggest that reverse shocks may be responsable for the flat emission registered in the first few hundreds seconds, while, from $\sim$500 s onwards, the optical and X-ray emission are produced by the same mechanism, possibly due to the forward shock as previously discussed.

4.2 The X-ray afterglow

Regardless of the interpretation of the third flare, after the second orbits (i.e. 5000 s after the trigger) *Swift* observed the X-ray afterglow of GRB 050712 and detected a break in the decay slope. We find that the values of two decay indices as well as the break time are weakly dependent on the exact start of the afterglow.

The initial shallow decay ($\alpha \approx -0.73$) and the break could be explained either by a late, continuous energy injection from the inner engine (Zhang & Mészáros 2001, 2002b), or, alternatively, by a model in which the central engine activity is as brief as the prompt emission itself but, at the end of the prompt phase, the ejecta are released with different Lorentz factors (Panaitescu et al. 2005). The two scenarios are observationally indistinguishable, although the second one reconciles better with the scenario of the onset of the afterglow at the third peak, as we will see in the following.

In the first case, a source luminosity law of the kind $L \propto t^q$ is assumed, where t is the intrinsic time of the central engine (or the

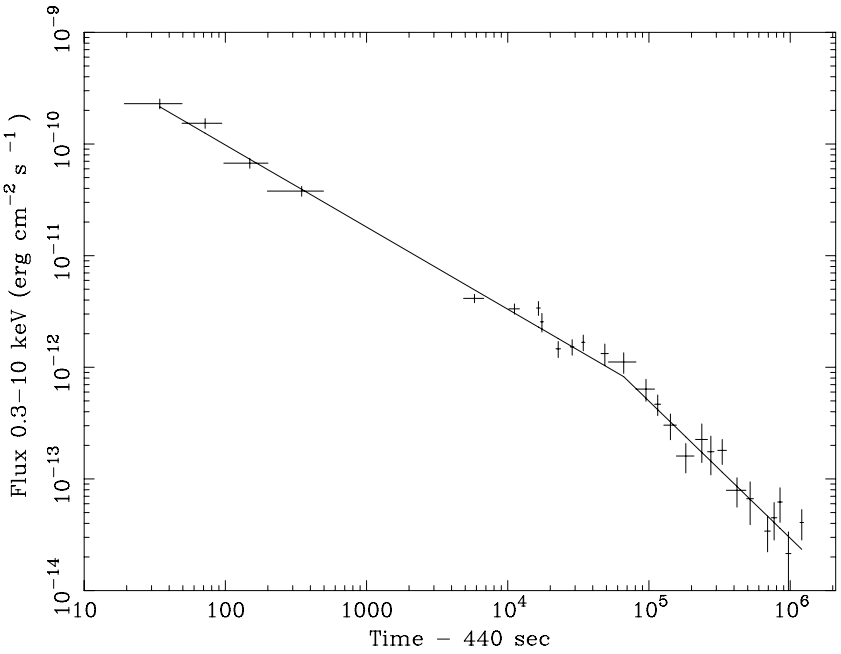

Figure 5. A broken power-law fit of the *Swift* XRT light curve of GRB 050712, computed assuming $t_0 = 440$ s (see text for details).

observer's time after the cosmological time dilation correction). Following (Zhang & Mészáros 2001, 2002b), the spectral and decay slopes are linked through the relation

$$\alpha = \left(1 - \frac{q}{2}\right)\beta + q + 1. \quad (4)$$

For the values of the indices we have before the break, we obtain $q \sim -0.5$. After the break, we get $q \sim -1$. In the continuous energy injection scenario, the former case indicates that the central engine produces a substantial amount of energy, which affects the fireball evolution. Instead, for $q \sim -1$, the energy which is added is small compared to the energy already injected and it does not affect the fireball evolution, effectively.

In the second scenario, the fastest shells initiate the forward shock, decelerate, and are successively caught by the slowest shells. The consequent addition of energy in the blast-wave mitigates the deceleration and the afterglow decay rate. Assuming that the mass M of the ejecta follows the law

$$M(>\gamma) \propto \gamma^s, \quad (5)$$

where γ is the Lorentz factor, the spectral and decay slope must be linked through the relationship (Zhang et al. 2006):

$$s = \frac{-(10 + 7q)}{2 - q}. \quad (6)$$

The degeneracy of the two models consists in the fact that a non-vanishing s index mimics the same effect of non-vanishing q index, although the physical mechanisms involved are different.

From the values of q reported above, we obtain $s = -2.6$ before the break and $s = -1$ after the break. Before the break time, the fast shells are decelerated initially with the slow shells lag behind ballistically and, when the fast ones are delerated enough, they are catch up by the slow shells. It is such pileup that gives an efficient conversion of energy: a steep distribution of the shells is required in order to have a significant energy injection into the blast wave, with more energy carried by slow shells. On the other hand, if the Lorentz factor distribution is flatter than $\simeq -1$, the injected energy is much smaller than that already present in the blastwave, so that the fireball dynamics is unaffected, and the afterglow enters the 'normal decay" phase.

4.3 Absorption by the circumburst medium

There is a general, growing, evidence for the association of long GRBs with the death of ultramassive stars (Galama et al. 2000; Hjorth et al. 2003; Stanek et al. 2003; Zeh, Klose & Hartmann 2004). Since these objects have a short lifetime ($\sim 10^6$ yr), it is expected that GRB explosions take place close to or inside the original star forming regions, where a dense circumburst medium is present. Thus, high level of absorption is expected, and this is consistent with the observations in ($\sim$50 per cent) of *Swift* bursts (Campana et al. 2005; O'Brien et al. 2005).

In order to verify the presence of an extragalactic absorber, we have first fitted the X-ray data with an absorbed power-law model, by keeping the absorption fixed at the Galactic value of $N_{\rm H}^{\rm Gal} = 0.13 \times 10^{22}$ cm^{-2} (Dickey & Lockmann 1990). This gives $\chi^2_\nu = 26.95/24$, $38.84/26$ and $13.1/16$ for the WT data taken during the first and second flare, the WT data taken after the second flare, and the PC data taken during the third flare, respectively. Later data have not been included in this analysis, because their statistics is quite poor. We then repeated the fit by adding an extra absorption component, and fixing the redshift at $z = 1$. We obtain $\chi^2_\nu = 21.5/23, 37.3/25$ and $12.10/15$, for the same three segments. We have calculated the probability of a chance improvement by means of the F-test (see, however, Protassov et al. 2002). We get $P = 0.02$, 0.20 and 0.28. Very similar results have been obtained by varying the redshift from $z = 0.5$ to 2. Results of the fits have been reported in Table 1. Therefore, data give a marginal indication for some intrinsic absorption for GRB 050712, at least in the first interval. Assuming a putative redshift $z = 1$, the value of the excess column density would be $N_{\rm H} = 5.6^{+2.4}_{-2.1} \times 10^{21}$cm^{-2}, $N_{\rm H} = 1.88^{+1.79}_{1.15} \times 10^{21}$cm^{-2} and $N_{\rm H} = 1.65^{+2.01}_{-1.00} \times 10^{21}$ cm^{-2}: there could be some indication of a decreasing column density, although all these values are also consistent with $N_{\rm H} \sim 3 \times 10^{21}$ cm^{-2}.

5 CONCLUSIONS

We presented *Swift* observations of the GRB 050712 and we discussed the properties of its optical and X-ray afterglows. The X-ray light curve of this burst does not decay immediately after the high-energy event, but it shows two episodes of flares in the first ∼1000 s. We find that the first and second flare is likely to be explained in terms of late internal shock emission. However, this might be not the case for the third flare. The different interpretation is based on the fact that during the third rise of the X-ray flux, the XRT spectrum is different from that detected during the previous phases, and more similar to that observed at the late afterglow epochs. Furthermore, the flux of the 'flare' can be connected with the late afterglow light curve with a broken power-law model, if the zero time is rescaled to the time of the onset of the peak. This is what is expected if the ejecta have been crossed by the reverse shocks, roughly at a time similar to that of the burst duration, and the onset of the external shock follows. Moreover, after the epoch of the third flare we observe a steepening of the optical-to-X-ray spectral index, $\beta_{\rm OX}$. This would suggest an increase in the optical emission, perhaps due to the contribution of the starting forward shock running in the circumburst medium. $\beta_{\rm OX}$ takes the value that will have for the remaining afterglow from this epoch. Although an internal shock interpretation cannot be completely ruled out, all these findings may also suggest that the last 'peak' represents the beginning of the standard afterglow phase.

The spectral fit also suggests some hints of intrinsic absorption, at least in the first ∼300 s. Assuming $z = 1$, the value would be $\sim 3 \times 10^{21}$ cm^{-1}, which is in the range of values for dense giant molecular clouds. If real, this finding is consistent with the idea of massive progenitors for GRBs. We cannot firmly establish whether or not the column density decreases at later times (e.g. by progressive ionization); we only note that, if the intrinsic absorption is not changing, it implies that the absorbing medium should not be very close to the place where the GRB took place (Lazzati & Perna 2002).

The fit presented in Fig. 5 shows that, up to ∼80 ks, the observed decay slope is rather shallow, with a slope $\alpha_1 \simeq -0.73$. This might be explained if a residual, continuous energy injection from the inner engine lasted at late times, with a luminosity law $L \propto t^{-0.5}$. A different explanation, that does not require a late-time reactivation of the central engine, is that ejecta are released with different Lorentz factor according to the distribution $M(>\gamma) \propto \gamma^{-2.6}$ (Zhang et al. 2006; Panaitescu et al. 2005). The decay slope observed after the break, $\alpha_2 \simeq -1.23$ is instead close to the standard decay slope observed in X-ray afterglows ∼1 day after the γ-ray event (De Pasquale et al. 2005; Gendre et al. 2005; Nousek et al. 2006; Zhang et al. 2006).

The constraint to the redshift ($z \leqslant 3$) enables us to set an upper limit on the energy emitted in γ-ray and X-rays by GRB 050712. If we assume $z = 3$ (which is *the* upper limit), and a spectral shape with low-energy spectral index −0.5, typical break energy of $E_0 =$ 300 keV and high-energy slope $= -1.5$, the k-corrected 1–10 000 keV energy emitted by GRB 050712 is 2.9×10^{53} erg.

ACKNOWLEDGMENTS

We are grateful to an anonymous referee for his/fer suggestions that led to a substantial improvement of the draft. SZ also thanks PPARC for support through an Advanced Fellowship.

REFERENCES

Barthelmy S. D. et al., 2005, Space Sci. Rev., 120, 143
Berger E. et al., 2003, Nat, 426, 154
Bloom J. S. et al., 1999, Nat, 401, 453
Burrows D. N. et al., 2005a, Space Sci. Rev., in press
Burrows D. N. et al., 2005b, X-ray Universe 2005 proceedings, preprint (astro-ph/0511039)
Campana S. et al. 2005, A&A, submitted
De Pasquale M. et al., 2005, A&A, submitted (astro-ph/0507708)
Dickey J. M., Lockman F. J., 1990, ARA&A, 28, 215
Esin A. A., Blandford R., 2000, ApJ, 534, L51
Falcone A. et al., 2005a, GCN 3573
Falcone A. et al. 2005b, ApJ, submitted
Frontera F. et al., 2004, ApJ, 614, 301
Galama T. J. et al., 2000, ApJ, 536, 185
Galli A., Piro L., 2005, A&A, in press (astro-ph/0510852)
Garnavich P., Loeb A., Stanek K., 2000, ApJ, 544, L11
Gehrels N. et al., 2005, ApJ, 621, 558
Gendre B., Corsi A., Piro L., 2005, A&A, in press (astro-ph/0507710)
Grupe D. et al., 2005a, GCN 3573
Grupe D., Burrows D., Morris D., Falcone A., Nousek J., Mészáros P., Chester M., Gehrels N., 2005b, GCN 3579
Hill J. E. et al., 2004, Proc. SPIE, 5165, 217
Hjorth J. et al., 2003, Nat, 423, 847
Huang Y. F., Wu X. F., Dai Z. G., Ma H. T., Lu T., 2004, ApJ, 605, 300
Kobayashi S., 2000, ApJ, 283, 694
Kumar P., Panaitescu P., 2000, ApJ, 541, L51
Kumar P., Piran A., 2000, ApJ, 541, L9
Lamb D. Q., 2003, AIP Conf. Proc. Vol. 662, Gamma-Ray Burst and Afterglow Astronomy 2001. Am. Inst. Phys., New York, p. 433
Lamb D. Q., Reichart D. E., 2000, ApJ, 536, 1L
Lazzati D., Perna R., 2002, MNRAS, 330, 383
Markwardt G. et al., 2005, GCN 3576
Maiorano E. et al., 2005, GCN 3601
Mészáros P., Rees M. J., 1997, ApJ, 476, 232
Nousek J. et al., 2006, ApJ, 642, 389
O'Brien P. et al., 2005, ApJ, in press (astro-ph/0601125)
Panaitescu A., Mészáros P., Rees M. J., 1998, ApJ, 503, 314
Panaitescu A., Mészáros P., Gehrels N., Burrows D., Nousek J., 2005, MNRAS, 366, 1357
Preece R. D. et al., 2000, ApJS, 126, 19
Piro L. et al., 2005, ApJ, 623, 314
Protassov R., van Dyk D. A., Connors A. et al., 2002, ApJ, 571, 545
Reichart E., 1999, ApJ, 521, L111
Rol E. et al., 2005, GCN 3575
Romano P. et al., 2006, A&A, 450, 59
Roming P. et al., 2005, Space Sci. Rev., in press
Sari R., Piran T., 1999, ApJ, 519, L17 (SP99)
Stanek K. Z. et al., 2003, ApJ, 591, L17
Zeh A., Klose S., Hartmann D. H., 2004, ApJ, 609, 952
Zeh A. et al., 2005, GCN 3646
Zhang B., Kobayashi S., 2005, ApJ, 628, 315
Zhang B., Mészáros P., 2001, ApJ, 552L, 35
Zhang B., Mészáros P., 2002a, ApJ, 581, 1236
Zhang B., Mészáros P., 2002b, ApJ, 566, 712
Zhang B., Mészáros P., 2004, IJMPA, 19, 2385
Zhang B., Kobayashi S., Mészáros P., 2003, ApJ, 595, 950
Zhang B., Fan Y. Z., Dyks J., Kobayashi S., Mészáros P., Burrows D. N., Nousek J. A., Gehrels N., 2006, ApJ, 642, 354
Zuo L., Lu L., 1993, ApJ, 418, 601

This paper has been typeset from a TEX/LATEX file prepared by the author.